



# Data-driven models for flood prediction in an ungauged karst wetland: Napahai wetland, Yunnan, China

Xiao Li<sup>1</sup> and Jie Li<sup>2,3</sup>

<sup>1</sup>School of Statistics and Mathematics, Yunnan University of Finance and Economics, Kunming, Yunnan, China

<sup>2</sup>Institute of International Rivers and Eco-security, Yunnan University, Kunming, Yunnan, China

<sup>3</sup>Yunnan Key Laboratory of International Rivers and Transboundary Eco-security, Yunnan University, Kunming, Yunnan, China

## ABSTRACT

Flood prediction for ungauged karst wetland is facing a great challenge. How to build a wetland hydrological model when there is a lack of basic hydrological data is the key to dealing with the above challenge. Napahai wetland is a typical ungauged karst wetland. In ungauged wetland/condition, this article used the wetland open water area (OWA) extracted from Landsat remote sensing images during 1987–2018 to characterize the hydrological characteristics of Napahai wetland. The local daily precipitation in the 1987–2018 rainy season (June–October) was used to set the variables. Based on the following hypothesis: in the rainy season, the OWA of the Napahai wetland rises when there is an increase in accumulated precipitation (AP), two data-driven models were established. The study took the area difference (AD) between two adjacent OWAs as the dependent variable, the accumulated precipitation (AP) within the acquisition time of two adjacent OWAs, and the corresponding time interval (TI) of the OWA as explanatory variables. Two data-driven models (a piecewise linear regression model and a decision tree model) were established to carry out flood forecasting simulations. The decision tree provided higher goodness of fit while the piecewise linear regression could offer a better interpretability between the variables which offset the decision tree. The results showed that: (1) the goodness of fit of the decision tree is higher than that of the piecewise linear regression model (2) the piecewise linear model has a better interpretation. When AP increased by 1 mm, the average AD increased by 2.41 ha; when TI exceeded 182 d and increased by 1 d, the average AD decreased to 3.66 ha. This article proposed an easy decision plan to help the local Napahai water managers forecast floods based on the results from the two models above. In addition, the modelling method proposed in this article, based on the idea of difference for non-equidistant time series, can be applied to karst wetland hydrological simulation problems with data acquisition difficulty.

Submitted 12 April 2022  
Accepted 1 February 2023  
Published 14 March 2023

Corresponding author  
Jie Li, [jli\\_1984@hotmail.com](mailto:jli_1984@hotmail.com)

Academic editor  
Alban Kuriqi

Additional Information and  
Declarations can be found on  
page 16

DOI 10.7717/peerj.14940

© Copyright  
2023 Li and Li

Distributed under  
Creative Commons CC-BY 4.0

OPEN ACCESS

**Subjects** Ecosystem Science, Natural Resource Management, Ecohydrology, Spatial and Geographic Information Science

**Keywords** Karst wetlands, Flood prediction, Open water area, Accumulated precipitation, Piecewise linear model, Decision tree

## INTRODUCTION

Floods are one of the most devastating disasters, causing about 620 billion US\$ of economic and property losses each year (Koks, 2018). Nearly half of the world's population lives around rivers, lakes, and wetlands, which are at a high risk of being affected by floods (Jongman, 2018). Karst wetlands have been widely developed around the world (Sullivan et al., 2014), and floods occur frequently (Hill & Polyak, 2020). Due to the complex hydrological interaction mechanism formed by groundwater and surface water on the dissolution and precipitation of soluble rocks, erosion and deposition, as well as gravity collapse, accumulation, etc., its flood disaster is unpredictable (Bates et al., 2021). In the current situation of frequent extreme climates, it is easier to expand the losses and impacts caused by such disasters, which is one of the main problems faced by the current natural disaster forecast and management (Noone et al., 2017; Blöschl et al., 2019).

The Yunnan-Guizhou Plateau in southwest China has developed a large number of karst landform units, and many areas have no features of surface water at all (Guo et al., 2013). If cracks or pipes in the limestone do not drain recharge quickly enough during heavy or prolonged rainfall, it can cause groundwater to overflow from the pipe network above ground, creating wetlands in low-lying areas (Drew, 2008; Hill & Polyak, 2020). In addition, under the influence of the monsoon climate, the precipitation in the rainy season is relatively concentrated, and it is easy to form a large area and periodic wetland flooding (Long et al., 2014). The Napahai Karst Wetland, also located in the northwestern part of Yunnan, China, has suffered repeated floods over the past 20 years, and many roads and houses in natural villages have been submerged, causing great economic losses. The reason for this is the rapid accumulation of water in low-lying areas of the catchment caused by continuous high-intensity rainfall (Li et al., 2013). How to predict the flooding of Napahai karst wetlands efficiently and accurately is a key issue in current flood management.

Current modeling methods for karst wetland hydrology can be divided into three broad categories (Hartmann et al., 2014; Basu, Morrissey & Gill, 2022): physics-based distributed hydrodynamic models, data-driven models, and the semi-distributed models between the two categories above (Ghasemizadeh et al., 2012; Kovács & Sauter, 2007). Among them, distributed and semi-distributed hydrodynamic models can simulate detailed hydrological processes by defining hydraulic parameters and system states, and they perform very well in simulating groundwater-surface water interactions in karst basins (Abusaada & Sauter, 2013; Gill et al., 2020; Hartmann et al., 2014). However, they have higher requirements for multi-level data and information (Chen & Goldscheider, 2014; Gill et al., 2013). For karst areas, it is difficult to simulate and restore the unique hydrological structures such as underground rivers and karst caves, which is the basis for applying distributed and semi-distributed hydrodynamic models based on physical processes. Thus, the value of such highly parameterized models is a recurrent debate in hydro(geo)logy (Beven, 2006). For the Napahai karst wetlands lacking basic hydrological monitoring such as water level monitoring, the above models are not ideal for flood forecasting.

In recent years, data-driven models for hydrological prediction of karst wetlands have mainly focused on machine learning methods. For example, Al-Fugara et al. (2020) and

*Naghibi, Ahmadi & Daneshi (2017)* compared the predictive power of several different machine learning methods for spatial mapping of groundwater potential. *Kurtulus & Razack (2007)* and *Lee & Tuan Resdi (2016)* used meteorological data such as precipitation to simulate water output through neural network modeling. *Guzman, Paz & Tagert (2017)* used historical data on precipitation and groundwater levels to predict future groundwater levels; *Wunsch, Liesch & Broda (2018)* used precipitation and air temperature to predict groundwater levels. The modeling methods of the latter two are also neural networks. *Basu, Morrissey & Gill (2022)* used both nonlinear time series and support vector machine methods for karst flood forecasting. The main advantage of machine learning methods is that they usually have a good prediction accuracy without understanding in depth the hydrological mechanism (*ASCE, 2000a; ASCE, 2000b*); the disadvantage is that the output results do not provide any model expression, which is an added challenge for outcome interpretability (*Lee & Tuan Resdi, 2016*).

Moreover, in order to obtain high goodness of fit, data-driven models usually need abundant data for model construction and validation. However, ungauged karst wetlands, widespread all over the world, lack in basic hydrological monitoring, and are located in places where it is challenging to collect sufficient data to construct data-driven models (*Malagò et al., 2016*). Due to these challenges, it makes sense to construct models for flood prediction in these areas.

Previous hydrological studies in Napahai wetland have verified that there is a strong correlation between accumulated precipitation (AP) and the open water area (OWA) (*Li et al., 2015*), and the rainy season as the main rainfall period is the peak flood period of the wetland (please see the 'Overview of the study area' in the article). Therefore, this article assumes that the main cause of the wetland flood, which means that the OWA of the wetland increases excessively, is caused by excessive AP in this region in a period of time. Establishing a hydrological statistical model based on the variation of AP and the OWA in the rainy season is helpful to reveal the hydrological regulation of Napahai karst wetland.

After comparing the prediction accuracy of different machine learning methods, this article selects the decision tree method. At the same time, considering the shortcomings of poor interpretability of machine learning methods, combined with the acquisition characteristics of hydrological data in the Napahai wetlands, we provide another method: the piecewise linear regression model. This article attempts to use precipitation and remote sensing data to predict Napahai wetlands floods by using a decision tree and a piecewise linear regression model, and to provide theoretical support for local flood management in terms of prediction accuracy and interpretability.

## MATERIALS & METHODS

### Overview of the study area

The Napahai watershed is a semi-closed watershed in the Hengduan Mountains on the southern margin of the Qinghai-Tibet Plateau (*Fig. 1*). The wetland is located at the end of the watershed, covering an area of nearly 30 km<sup>2</sup>. Water comes from the Nachi river, Dalangchi river, Naizi river, dozens of mountain streams and outcropping springs, and the

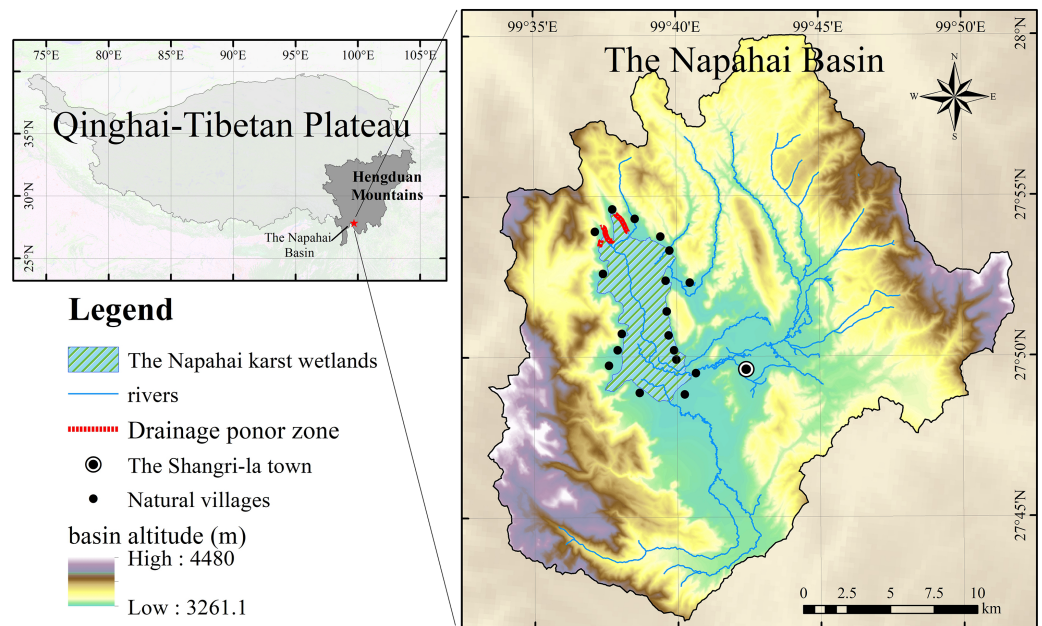


**Figure 1** The location of the Napahai karst wetland and its basin.

Full-size DOI: [10.7717/peerj.14940/fig-1](https://doi.org/10.7717/peerj.14940/fig-1)

groundwater flows into the wetlands (*Li et al., 2013*). They are connected by a small water network together and form a complex wetland structure. Then, the water flows out to the tributaries of the Jinsha river, through the karst seepage layer distributed in the northern part of the wetlands.

Affected by the monsoon climate, the distribution of precipitation in the Napahai Basin is extremely uneven during the year. The precipitation from May to October accounts for about 85% of the annual precipitation, while the precipitation from November to the following April accounts for only 15% of the annual precipitation. The large difference in annual precipitation causes significant seasonal fluctuations in the open water surface of the wetland. The concentrated rainfall in summer is the main reason for the rapid expansion of the open water surface of the Napahai wetlands (*Li et al., 2015*). According to the statistics of the local management department, when the OWA of the wetland exceeds 1844.76 ha, the farmland will be submerged and the surrounding area will be affected. This OWA can be defined as the area threshold for flood disasters in the Napahai wetlands.

According to previous research on the Napahai wetlands, since 2000, the OWA has exceeded 1844.76 ha four times. The OWA of the Napahai Wetland in the rainy season of 2018 reached 2573.57 ha, which caused disasters to 518 surrounding residents, submerged farmland for 162 ha, causing great property losses (*Napahai Nature Reserve Administration, 2020*).

At present, due to the lack of long-term regular hydrological monitoring, such as the main river flow and water level data, only the measured data such as precipitation and the OWA data interpreted from remote sensing images can be used in the flood prediction and simulation of the Napahai Wetlands.

## Research approach

This article aims to predict the OWA by daily precipitation data of the Napahai wetland during the rainy season (May–October) from 1987 to 2018 so as to achieve the purpose of flood prediction. The reason why only the rainy season data is considered here is because the rainy season in the summer is the main source of flooding in the Napahai wetland. An OWA is predicted instead of a wetland water level due to the fact that the conventional water level data cannot be obtained, but remote sensing image data can provide OWA data.

A total of 47 OWA data of the Napahai wetland during the rainy season can be used from 1987–2018, which has the characteristic of non-equidistant time series. The routine modelling methods such as ARMA (autoregressive moving average model), ARIMA (autoregressive integrated moving average model), *etc.*, for the usual equidistant time series data cannot be applied here, but we could still borrow the idea of difference to deal with time series data. The reason why time series modelling needs to be done by difference operation is to avoid the pseudo-correlation caused by non-stationary time series. The difference in two adjacent OWA is related to the AP between the two observations and might also be related to the time interval (TI) of the two observations. Thus, we obtained the dependent and independent variables and Fig. 2 provides the data flow acquisition for the variables.

In this article, AP and TI are used to predict the difference of OWA, and the piecewise linear regression and decision tree methods are selected. The reason for choosing the piecewise linear model is based on the descriptive analysis followed that discovers that the OWA difference has a piecewise linear relationship with TI. The decision tree is chosen because it is the most accurate method to predict this data set among the most common machine learning methods such as random forest, neural network *etc.* after comparing them.

## Original data and preprocessing

(1) Extracting the Open Water Surface (OWS) of the Napahai Wetland through Landsat imageries

To ensure the consistency of data spatial accuracy, the remote sensing data used in this study are all Landsat TM (thematic mapper)/ETM+ (enhanced thematic mapper plus)/OLI (operational land imager) data. The data sources are: China Remote Sensing Data Network (<http://eds.ceode.ac.cn>) and USGS (United States Geological Survey) Image Database (<http://glovis.usgs.gov>).

A total of 47 Landsat images covering the Napahai wetlands with cloud cover less than 5% in the rainy season from 1987 to 2018 were collected. Among them, 30 scenes are Landsat4/5 TM, 6 scenes are Landsat7 ETM+ SLC (scan lines corrector)-on, three scenes are Landsat7 ETM+ SLC-off, and eight scenes are Landsat8 OLI (as shown in Table 1). We performed the geometric correction (the datum is WGS-84, UTM projection zone 47N) and radiometric correction for all image data. The modified normalized difference water index (MNDWI) method was used to interpret and extract the OWS of the wetlands to obtain its OWA in different periods. Some studies have shown that the MNDWI method can stably and effectively identify the open water landscape (Xu, 2006). The calculation

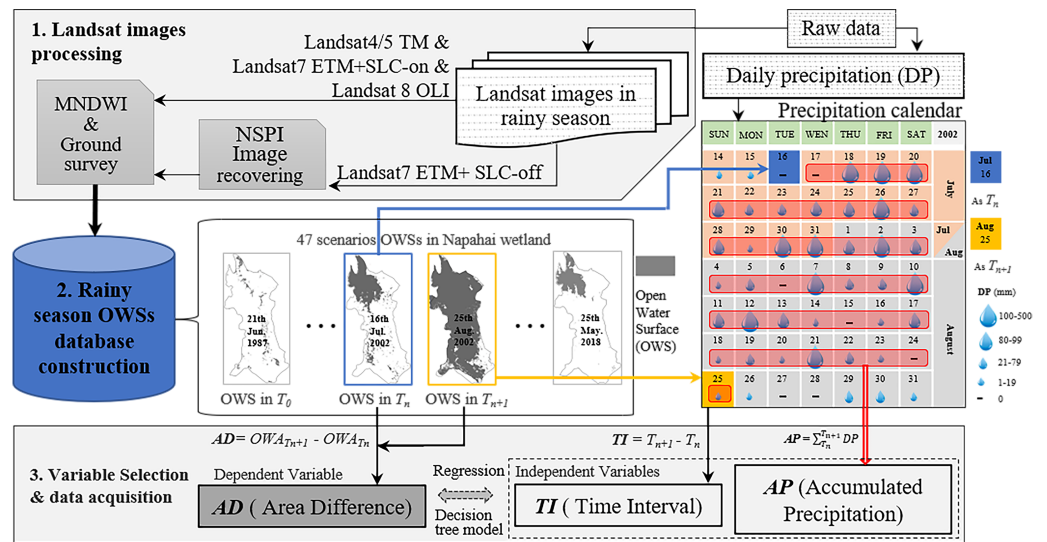


**Figure 2** The flowchart of how the variables acquired from the Landsat images and daily precipitation data. The first independent variable,  $TI$  represented the difference in days between the acquisition time of the  $N$ th image and the following image. For example, The  $TI$  between Aug 25 and Jul 16 in the precipitation calendar was 40 days. The second independent variable,  $AP$  represented the accumulated DP between  $T_n$  and  $T_{n+1}$ . The dependent variable,  $AD$  was calculated by the OWA different between the OWS in  $T_n$  and  $T_{n+1}$ . OWA is the area of OWS.

Full-size [DOI: 10.7717/peerj.14940/fig-2](https://doi.org/10.7717/peerj.14940/fig-2)

method is shown in Eq. (1):

$$MNDWI = \frac{Green - MIR}{Green + MIR}. \quad (1)$$

In Eq. (1), *Green* represents the green light band in remote sensing data; *MIR* represents the mid-infrared band in remote sensing data.

Furthermore, after May 31, 2003, the SLC on the Landsat 7 ETM+ airborne scan line corrector failed, and the subsequent images (*i.e.*, ETM + (SLC -off)) lost data stripes. In this study, all Landsat 7 ETM + (SLC -off) image data were repaired by the NSPI method (Chen et al., 2011; Li et al., 2015).

In order to improve the accuracy of remote sensing interpretation, this study carried out ground surveys at the same time according to the shooting time of remote sensing images. We used an RTK (Real Time kinematic) GNSS (Global Navigation Satellite System) to collect ground landscape information. A total of 4617 points were collected within the area (as shown in Fig. 3). The sampling point density is 146.6 points/km<sup>2</sup>. Within the collection of the landscape information and the surface features extracted by the MNDWI index, we determined the threshold for interpreting OWS and non-OWS as  $-0.31$ . The confusion matrix method was used to test the interpretation accuracy of the extracted OWS, the accuracy rate was 88.2%, the precision rate was 90.1%, and the Kappa coefficient was 0.76, indicating that the interpretation results were highly consistent with the real situation.

(2) The OWA of Napahai wetlands

**Table 1** Landsat-derived area of OWA in Napahai Wetlands in the rainy season.

ID	Time phase	Area (ha)	ID	Time phase	Area (ha)
1	1987-06-21	156.42	25	2005-05-29	66.03
2	1990-05-12	152.09	26	2005-09-10	1094.54
3	1990-06-13	321.24	27	2006-05-16	178.76
4	1992-06-02	232.97	28	2006-07-27	403.77
5	1992-08-05	721.11	29	2007-10-26	1676.63
6	1995-05-10	210.14	30	2008-07-08	214.83
7	1996-10-19	310.99	31	2008-10-12	1490.8
8	1997-05-15	62.18	32	2009-05-08	207.66
9	1997-09-20	1107.86	33	2009-07-19	480.69
10	1998-09-07	1639.57	34	2010-06-12	235.74
11	1999-08-01	683.8	35	2010-07-30	1598.12
12	2000-09-20	1729.45	36	2010-08-07	1968.66
13	2000-10-06	972.18	37	2011-05-06	912.15
14	2000-10-14	652.09	38	2011-08-10	715.88
15	2000-10-22	476.94	39	2011-09-27	462.87
16	2002-05-05	197.05	40	2013-05-27	215.46
17	2002-07-16	780.24	41	2013-08-15	323.28
18	2002-08-25	2680.3	42	2015-05-01	156.78
19	2002-09-20	2890.14	43	2016-05-03	477.18
20	2002-10-02	2221.29	44	2016-08-07	1739.25
21	2002-10-28	1809.9	45	2017-05-22	505.89
22	2003-06-01	122.9	46	2017-06-07	712.26
23	2004-07-05	330.71	47	2018-05-25	414.81
24	2004-09-15	1702.58		–	

The 47 scenarios of the Napahai Wetland OWA in the rainy season from 1987 to 2018 interpreted according to Landsat images are shown in [Table 1](#), where the sensor represents the different sensors carried by the series of Landsat satellites. In [Fig. 4](#), the OWA in the rainy season from 1987 to 2018 fluctuated greatly, and the largest OWA appeared in 2002.

### (3) Daily precipitation data

Napahai Wetland is close to Shangri-la, therefore we used the daily precipitation monitoring data from the Shangri-la meteorological station as the main data source.

The time series of annual precipitation and the average monthly precipitation of the wetland is shown in [Fig. 5](#). The annual maximum rainfall in the Napahai wetland occurred in 2002 with 854.1 mm, followed by 817.6 mm in 2000. The rainfall was intense in July and August and steady from November to April.

## Empirical model construction

### (1) Data transformation

After organizing the original data, we generated two variables that had a strong impact on area difference (AD): AP and TI. The description of each variable is shown in [Table 2](#), and the data for each variable are shown in [Table 3](#). TI depends on the acquisition time of

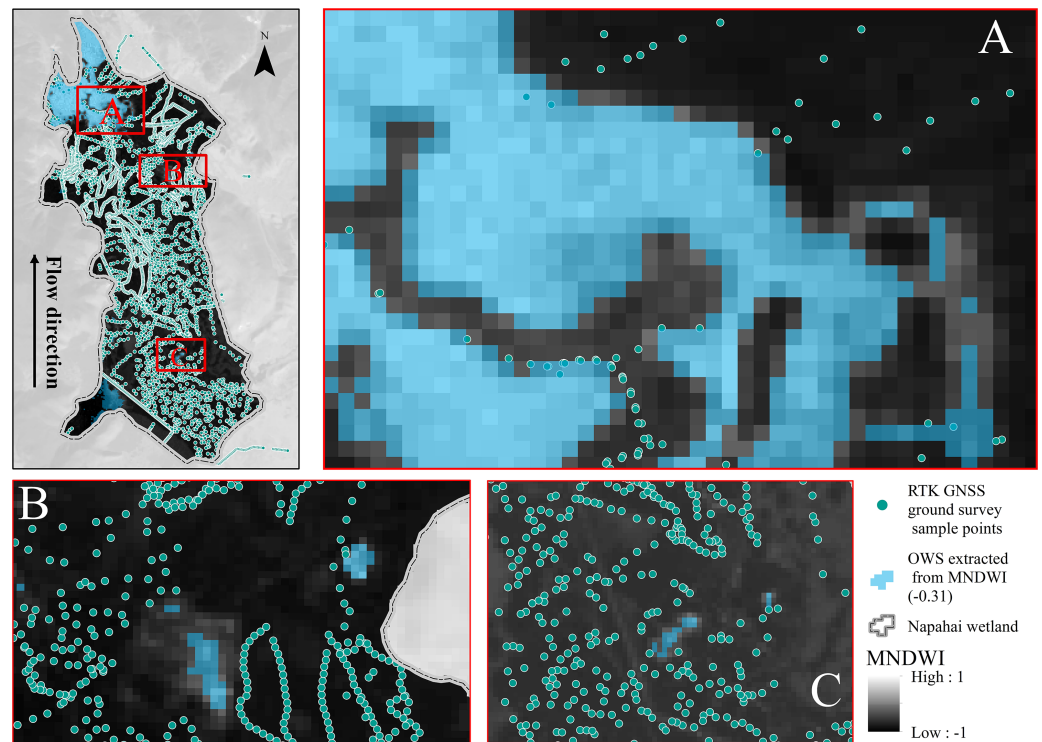


**Figure 3** Extracted open water surface (OWS) by MNDWI based on the Landsat imageries and the real-time ground survey to determine the OWS interpretation threshold value of  $-0.31$ . The MNDWI is a value between  $-1$  and  $1$ . With the 4,617 points RTK GNSS ground survey of OWS and non-water, when a pixel value was greater than  $-0.31$  in the research area, it would be identified as OWS.

Full-size [DOI: 10.7717/peerj.14940/fig-3](https://doi.org/10.7717/peerj.14940/fig-3)

**Table 2** Variable description of the difference data.

Variable type	Variable name (unit)	Value range	Description
Dependent variable	AD (ha)	$[-1687.00, 1900.05]$	According to the order of the observation time, the area difference of open water between two adjacent observations.
	AP (mm)	$[0, 1869.8]$	According to the order of the observation time, the sum of the daily precipitation of two adjacent observations.
Independent variables	TI (day)	$[8, 1056]$	According to the order of the observation time, the time interval between two adjacent observations.

**Notes.**

Abbreviations: AD, area difference; AP, accumulated precipitation; TI, time interval.

each remote sensing data point, and because the visible remote sensing data are strongly affected by cloud cover, the TI among some samples was relatively large.

(2) Descriptive analysis

In order to determine the effect of AP and TI on AD, we constructed the corresponding scatter plots, which are shown in Fig. 6. It was obvious that there was an approximately linear positive correlation between AP and AD, while the relationship between TI and



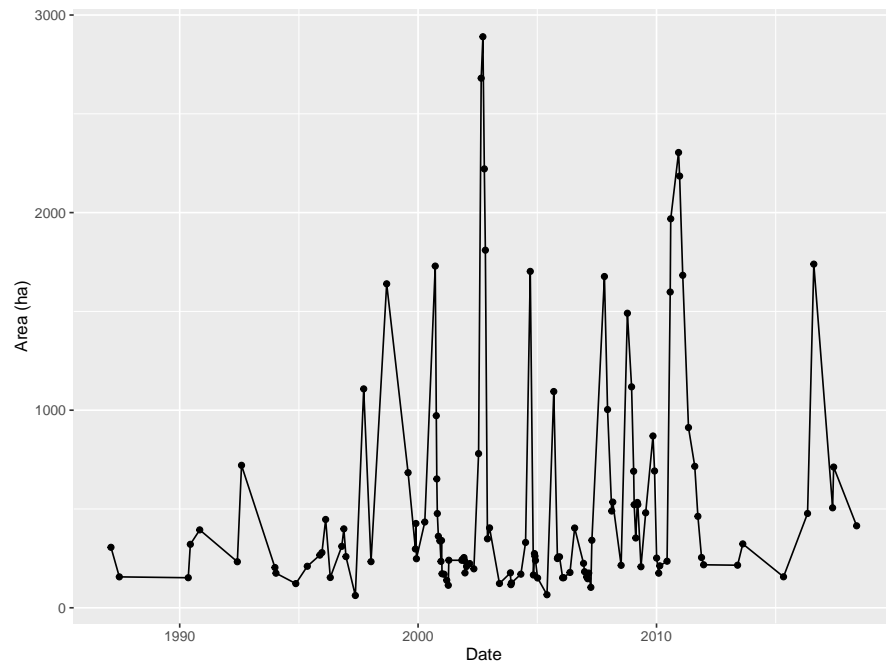


**Figure 4** Time series graph for open water area (OWA) from 1987 to 2018.

Full-size  DOI: 10.7717/peerj.14940/fig-4

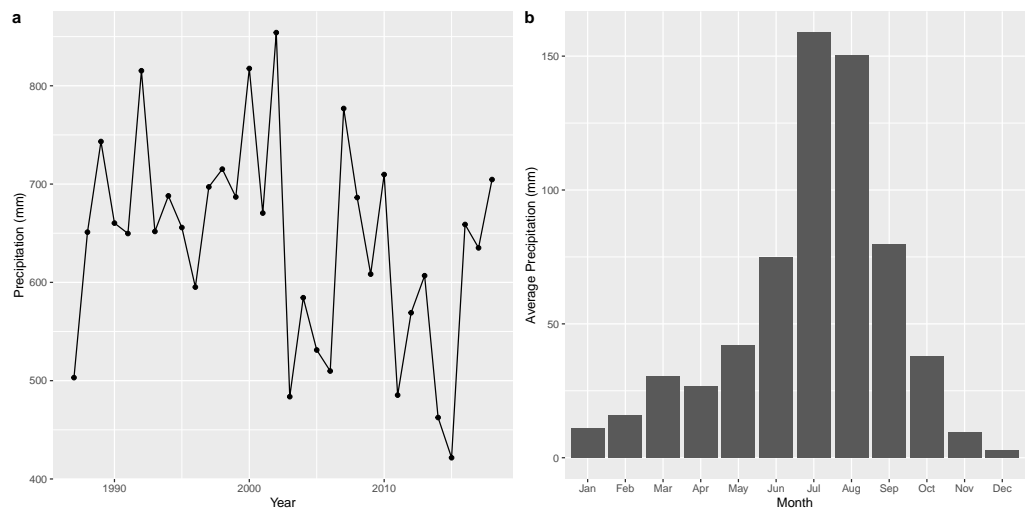


**Figure 5** Characteristic description for precipitation from 1987 to 2018.

Full-size  DOI: 10.7717/peerj.14940/fig-5

AD was somewhat complex, *i.e.*, a piecewise linear correlation, and the inflection point occurred at approximately 182 d.

### (3) Model selection

In theory, we can choose all kinds of models for model candidates here, such as the linear regression model, non-linear regression model and all kinds of machine learning methods.

**Table 3** The corresponding data of Table 2.

Time phase	AD (ha)	AP (mm)	TI (day)	Time phase	AD (ha)	AP (mm)	TI (day)
1987-06-21		–		2005-05-29	–1636.55	172.4	256
1990-05-12	–4.33	1869.8	1056	2005-09-10	1028.51	354.5	104
1990-06-13	169.14	98.4	32	2006-05-16	–915.78	137.6	248
1992-06-02	–88.27	1359.8	720	2006-07-27	225.01	251.4	72
1992-08-05	488.15	264.8	64	2007-10-26	1272.86	921.7	456
1995-05-10	–510.97	1792.8	1008	2008-07-08	–1461.80	310.4	256
1996-10-19	100.85	1170.5	528	2008-10-12	1275.97	349.9	96
1997-05-15	–248.81	86.5	208	2009-05-08	–1283.14	148.7	208
1997-09-20	1045.68	548.2	128	2009-07-19	273.03	208	72
1998-09-07	531.71	702.5	352	2010-06-12	–244.95	460.6	328
1999-08-01	–955.77	433.8	328	2010-07-30	1362.39	248.4	48
2000-09-20	1045.66	1098.6	416	2010-08-07	370.54	52.7	8
2000-10-06	–757.28	29	16	2011-05-06	–1056.51	329.4	272
2000-10-14	–320.08	0	8	2011-08-10	–196.27	268.6	96
2000-10-22	–175.16	0	8	2011-09-27	–253.01	117.2	48
2002-05-05	–279.89	779.2	560	2013-05-27	–247.41	692.5	608
2002-07-16	583.19	319.9	72	2013-08-15	107.82	293.4	80
2002-08-25	1900.05	335.4	40	2015-05-01	–166.50	748.1	624
2002-09-20	209.85	73	26	2016-05-03	320.40	452.4	368
2002-10-02	–668.85	50	22	2016-08-07	1262.07	378.2	96
2002-10-28	–411.39	8.9	16	2017-05-22	–1233.36	266.7	288
2003-06-01	–1687.00	93	216	2017-06-07	206.37	44.3	16
2004-07-05	207.81	626.8	400	2018-05-25	–297.45	584.2	352
2004-09-15	1371.87	918.5	72		–		

Based on descriptive analysis above, it can be observed that the linear regression model is inappropriate here, and the piecewise linear regression might be a reasonable model. For the machine learning methods, we tried the decision tree, bagging, random forests and support vector machines. In the end, we found that the simple method “decision tree” has the best prediction accuracy for this dataset. Regarding the comparison between the piecewise linear regression model and decision tree, they have different advantages and disadvantages. The details can be found in the section on the model comparison. In this article, we show the result details of the piecewise linear model and decision tree.

#### (4) Prediction accuracy

In order to evaluate a model’s prediction accuracy, we consider the following evaluation indicators.

Goodness of fit:  $R^2$

$$R^2 = \frac{\sum_{i=1}^n (\hat{y}_i - \bar{y})^2}{\sum_{i=1}^n (y_i - \bar{y})^2}. \quad (2)$$

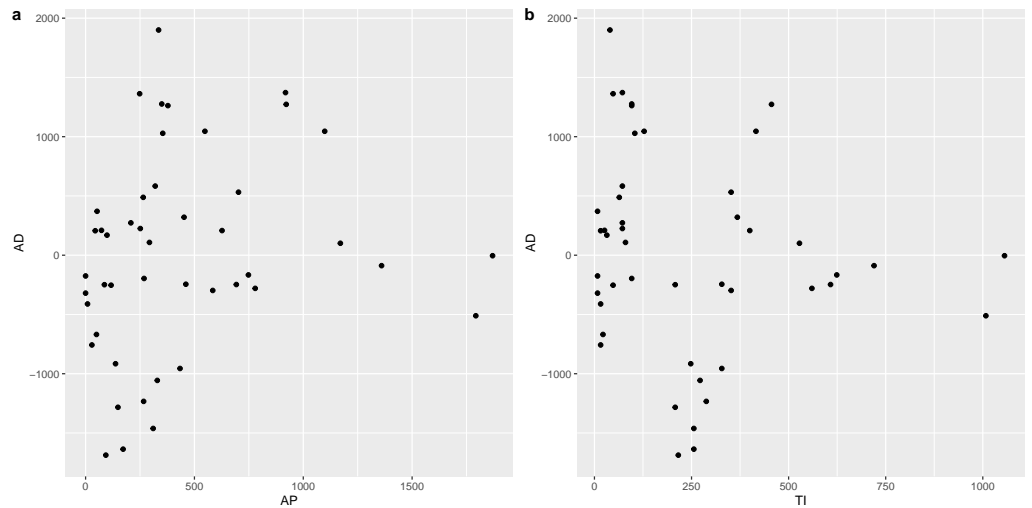


**Figure 6** Scatter plot between AP and AD, TI and AD respectively.

Full-size  DOI: [10.7717/peerj.14940/fig-6](https://doi.org/10.7717/peerj.14940/fig-6)

Adjusted  $R^2$ :

$$R_A^2 = 1 - (1 - R^2) \frac{n-1}{n-p-1}. \quad (3)$$

Mean Square Error:

$$MSE = \frac{1}{n} \sum_{i=1}^n (\hat{y}_i - y_i)^2. \quad (4)$$

Note  $n, p, y_i, \hat{y}_i$  represent the sample size, number of covariates,  $i$ -th observation of the dependent variable and its fitting value respectively.  $\bar{y}$  is the average value of all of the observations of the dependent variable.  $R^2$  is used to evaluate the fitting effect of the regression model; it ranges from 0 to 1, and a higher value indicates a better model fit. However, there is a tendency to encourage more explained variables even meaningless explained variables. The adjusted  $R^2$  makes up for the shortcoming (Rencher & Schaalje, 2008). The MSE will be small if the predicted responses are very close to the true responses and will be large if for some of the observations, the predicted and true responses differ substantially (James et al., 2013).

## RESULTS

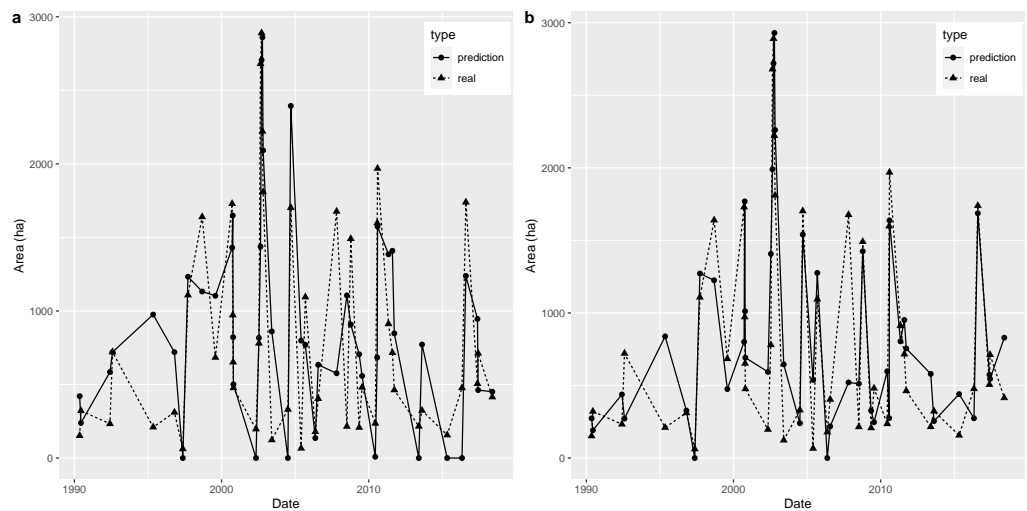
### Model results

It was observed that the relationship between AD and TI was segmented (see Fig. 6B), with 182 d (half a year) as the inflection point, and two linear regression models were established afterward, corresponding to the fitting of  $\leq 182$  d and  $> 182$  d. The results are shown in Table 4.

Table 4 shows that for every one mm increase in AP, AD increased by 2.41 ha, whether TI was longer or shorter than 182 d. This indicated that the impact of AP on AD was

**Table 4** Results for the linear regression model.

TI $\leq$ 182				TI $>$ 182			
Variable	Regression coefficients	P-value	Remark	Variable	Regression coefficients	P-value	Remark
Intercept	-150.73	0.36		Intercept	-382.56	0.25	
AP	2.41	<0.001		AP	2.41	0.004	
F test		<0.001	$R^2 = 0.51$	F test		<0.001	$R^2 = 0.43$

**Figure 7** (A–B) Prediction graph for the piecewise linear regression model and the decision tree.

Full-size  DOI: [10.7717/peerj.14940/fig-7](https://doi.org/10.7717/peerj.14940/fig-7)

independent of TI. In addition, when  $TI \leq 182$  d, TI had no significant effect on AD, and therefore it did not appear in the final model. When  $TI > 182$  d, TI had a significant negative correlation with AD, shown in Table 4; for every 1 d increase in TI, AD decreased by 3.66 ha.

Therefore, we predicted the AD value through the above model, and then used the nearest OWA extracted by remote sensing images to predict the OWA on a specific observation date. Based on a comparison of the predicted OWA and the extracted OWA, which are presented in Fig. 7A, we found a certain difference between the two series in general. However, the model produced a relatively accurate prediction for 2002, which was when the OWA reached the historical peak, therefore this model has a certain reference value for flood forecasting.

The results of the decision tree are shown in Fig. 8. In total, there were 46 samples, and the average AD was 5.62 ha. The whole data set was divided into two parts with a TI of 168 days as the dividing point. There were 23 samples whose TI was shorter than 168 days, and the corresponding average value of AD was 396 ha. When the AP was less than 307 mm, there were 16 samples, and the AD was predicted to be 39.4 ha. In contrast, when the AP exceeded 307 mm, the AD was predicted to be 1210 ha. There were 23 samples whose TI

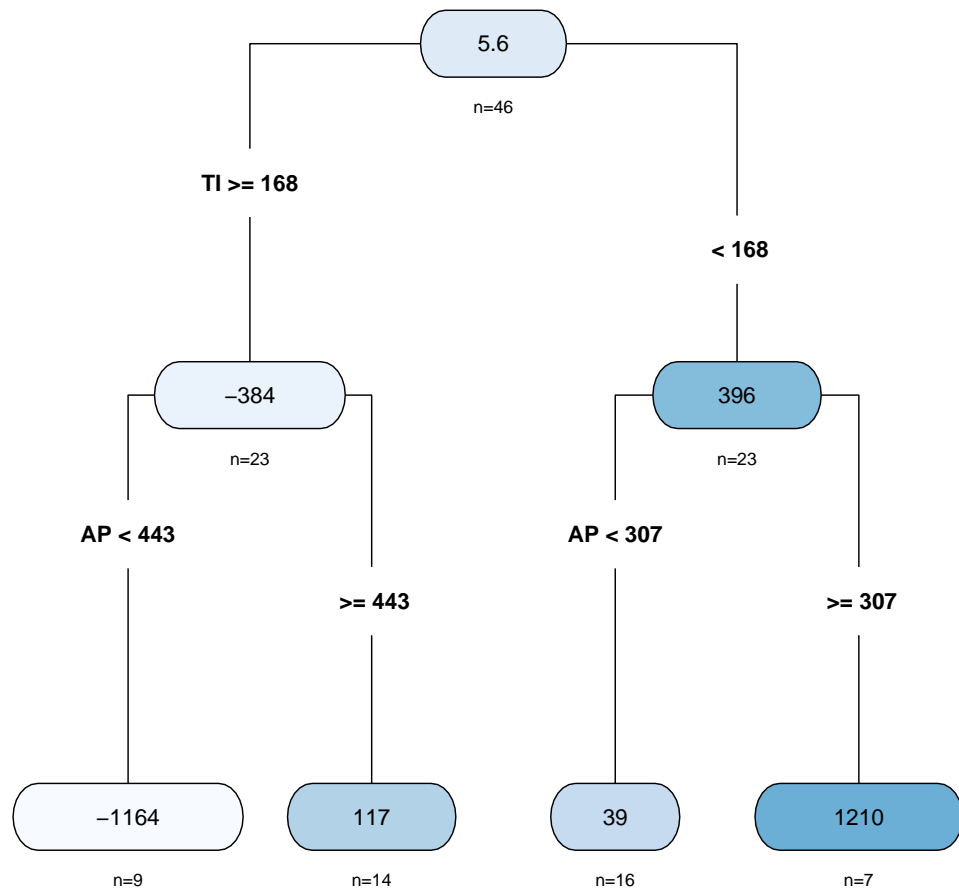


**Figure 8** The decision tree plot.

Full-size  DOI: [10.7717/peerj.14940/fig-8](https://doi.org/10.7717/peerj.14940/fig-8)

exceeded 168 days; the corresponding AD was  $-384$  ha; among them, only nine samples had AP values less than 443 mm, and the corresponding AD was predicted to be  $-1164$  ha; otherwise, it was predicted to be 117 ha.

The comparison between the OWA predicted by the decision tree model and the extracted OWA is shown in Fig. 7B (note: when the predicted value was negative, we set it to 0). Compared with the piecewise linear regression model, the accuracy of this method was relatively high. In addition, there was little difference between the predicted OWA and the extracted OWA for the largest flood in 2002, which means the decision tree model was accurate in terms of flood simulation.

## Model comparison

### (1) Comparison of prediction accuracy

The  $R^2$ , adjusted  $R^2$  and MSE results are shown in Table 5. Both the piecewise linear regression model and the decision tree have a moderate level of fitting effect. For example, the decision tree model could explain approximately 69% variation of the sample AD for this dataset. Both methods have relatively large MSE. There might be two reasons for that.

**Table 5** Comparison of model fitting effect.

	Piecewise linear regression	Decision tree
$R^2$	0.58	0.69
Adjusted $R^2$	0.56	0.68
MSE	411325.04	492566.04

First, both methods have difficulty in predicting all the observations accurately which yield large MSE. Second, the sample size is small, which is an added challenge for prediction accuracy. Obviously, the decision tree model has better  $R^2$ , adjusted  $R^2$  but worse MSE. We might understand the results in the way that the decision tree has less bias for this dataset, but the piecewise linear model is more robust here.

#### (2) Comparison of the interpretability of the models

Regarding the fitting results of the linear model, each regression coefficient has a definite meaning in practice. In particular, the piecewise linear regression coefficients in [Table 4](#) were explained before (see ‘Model results’ section) and are helpful for local managers in Napahai to understand how AP and TI influence AD. On the contrary, the decision tree is a type of machine learning method; its modelling is mainly based on an algorithm, and it is almost impossible to interpret its results.

In conclusion, the piecewise linear model has a relative lower prediction accuracy, but a better interpretability and robustness compared with the decision tree. Considering that they both have advantages and disadvantages, we chose to keep both methods as our final models.

## DISCUSSION

### Decision analysis

In order to help the water managers to predict the flood in the Napahai wetland, the article provides two schemes. The decision tree is better in terms of prediction accuracy, and the piecewise linear regression is better in terms of comprehensibility and robustness.

In fact, we can combine the two models’ results to give a simpler decision scheme. First, according to the decision tree, we verified whether AP is greater than 307 mm to make a preliminary judgment on the flood risk. If not, it is judged as low risk, otherwise it is high risk, and the manager needs to predict whether OWA will exceed 1844.76ha further based on the piecewise linear regression model.

### Limitations

In this article, the prediction analysis method has some limitations, mainly related to the following two aspects: (a) Prediction accuracy is not very high. The fundamental reason is the difficulty of data acquisition. Data access poses a challenge concerning other factors that may affect flood and equidistant OWA time series data. Data acquisition is one of challenges for Karst flood predictions ([Hartmann et al., 2014](#)). (b) This article only simulates the OWA of the Napahai wetland, and it will be better if it can be extended to the

two-dimensional open water distribution ([Wen et al., 2013](#); [Seleem et al., 2022](#)). We will consider this in the future when we can obtain more data.

### Comparison with similar studies

Precipitation is a core element of the terrestrial hydrological cycle, and therefore almost all studies related to hydrological simulation will use rainfall as the main variable of their models ([Ghasemizadeh et al., 2012](#); [Kovács & Sauter, 2007](#); [Basu, Morrissey & Gill, 2022](#)). From this point of view, this study is consistent with similar studies. Data-driven models are also widely used in research on flood prediction ([Guzman, Paz & Tagert, 2017](#); [Hadid, Duviella & Lecoeuche, 2020](#); [Sawaf et al., 2021](#)). Some studies have expressed the advantages of data-driven model compared with the physical model: it has fewer requirements for hydrological variables ([Ji et al., 2012](#); [Seleem et al., 2022](#)), which reflects in the model building that usually has data-lacking problems. Researchers tend to use precipitation, water level, discharge and other variables for modeling with sufficient data. However, when these data are insufficient, researchers are more inclined to use multi-source remote sensing data to obtain hydrological data such as OWS and so on ([Windolf et al., 2011](#); [Spence et al., 2013](#); [Yang, Cai & Wang, 2018](#)), which is similar to the method used in this study.

Moderate-resolution imaging spectroradiometer (MODIS) remote sensing data (with a high satellite replay period: 1d and relatively low spatial resolution: 250 m) are often used to extract the OWS of the ungauged wetland. The advantage of using MODIS as the data source is that it can obtain enough OWA data within a relatively long study period, which provided sufficient samples ([Gumbrecht et al., 2004](#)). The disadvantage is that, for relatively small wetlands, its low spatial resolution cannot accurately represent the pattern of the OWS.

In the studies of flood prediction modeling, machine learning methods were widely used. These studies gained fine prediction accuracy for the large amount of training samples ([Qian, Mohamed & Claudel, 2019](#); [Basu, Morrissey & Gill, 2022](#)). However, these studies still cannot quantitatively explain the impact of precipitation on flooding. Therefore, in addition to the machine learning model, the traditional regression model can make up for the disadvantages of the machine learning model, which is also the reason why this article maintains both models.

## CONCLUSIONS

This article described a piecewise linear regression model and a decision tree model to provide solutions for flood predictions of the Napahai wetland based on limited and non-equidistant time series data. We combined both methods to provide an easy effective risk management for flood prediction that makes a preliminary judgment of flood risk level based on whether AP is larger than 307 mm (decision tree result), and then check if OWA is larger than the flood threshold based on piecewise linear regression model if necessary.

## FUTURE WORK

(1) Obtaining multi-source remote sensing data (such as in recent years, constantly enrich the high-resolution optical remote sensing data, as well as microwave and radar remote

sensing data; among them, the latter can effectively reduce the influence of the monsoon cloud cover for remote sensing data acquisition), extract more OWA data of Napahai wetland, and increase the number of samples for the model, so as to improve the model accuracy. (2) If sufficient OWS data of the wetland are obtained, the spatial simulation of the flood could be modeled in Napahai karst wetland along with the local meteorological data, spatial feature statistics of the OWS and the terrain model of the wetland.

### **Index of Abbreviations and Notations**

#### **Abbreviations**

<b>OWA</b>	open water area
<b>AD</b>	area difference
<b>AP</b>	accumulated precipitation
<b>TI</b>	time interval
<b>ARMA</b>	autoregressive moving average model
<b>ARIMA</b>	autoregressive integrated moving average model
<b>OWS</b>	open water surface
<b>TM</b>	thematic mapper
<b>ETM+</b>	enhanced thematic mapper plus
<b>OLI</b>	operational land imager
<b>USGS</b>	United States geological survey
<b>MNDWI</b>	modified normalized difference water index
<b>RTK</b>	real time kinematic
<b>GNSS</b>	global navigation satellite system

#### **Notations**

<b>d</b>	day
<b>ha</b>	hectare

## **ADDITIONAL INFORMATION AND DECLARATIONS**

### **Funding**

This work was supported by the National Natural Science Foundation of China (No. 41601060). The funders had no role in study design, data collection and analysis, decision to publish, or preparation of the manuscript.

### **Grant Disclosures**

The following grant information was disclosed by the authors:  
National Natural Science Foundation of China: 41601060.

### **Competing Interests**

The authors declare there are no competing interests.



## Author Contributions

- Xiao Li conceived and designed the experiments, performed the experiments, analyzed the data, prepared figures and/or tables, authored or reviewed drafts of the article, and approved the final draft.
- Jie Li conceived and designed the experiments, performed the experiments, analyzed the data, prepared figures and/or tables, authored or reviewed drafts of the article, and approved the final draft.

## Data Availability

The following information was supplied regarding data availability:

The Open Water area data is packaged in a geodatabase (that can be opened by using ArcGIS software), and Daily precipitation data, are available in the [Supplemental Files](#).

## Supplemental Information

Supplemental information for this article can be found online at <http://dx.doi.org/10.7717/peerj.14940#supplemental-information>.

## REFERENCES

- Abusaada M, Sauter M. 2013.** Studying the flow dynamics of a karst aquifer system with an equivalent porous medium model. *Ground Water* 51(4):641–650.
- Al-Fugara A, Pourghasemi HR, Al-Shabeeb AR, Habib M, Al-Adamat R, Al-Amoush H, Collins AL. 2020.** A comparison of machine learning models for the mapping of groundwater spring potential. *Environmental Earth Sciences* 79:Article 206 DOI 10.1007/s12665-020-08944-1.
- ASCE Task Committee on Application of Artificial Neural Networks in Hydrology. 2000a.** Artificial neural networks in hydrology. I: preliminary concepts. *Journal of Hydrologic Engineering* 5(2):115–123.
- ASCE Task Committee on Application of Artificial Neural Networks in Hydrology. 2000b.** Artificial neural networks in hydrology. II: hydrologic applications. *Journal of Hydrologic Engineering* 5(2):124–137.
- Basu B, Morrissey P, Gill LW. 2022.** Application of nonlinear time series and machine learning algorithms for forecasting groundwater flooding in a lowland karst area. *Water Resources Research* 58:e2021WR029576 DOI 10.1029/2021WR029576.
- Bates PD, Quinn N, Sampson C, Smith A, Wing O, Sosa J, Savage J, Olcese G, Neal J, Schumann G, Giustarini L, Coxon G, Porter JR, Amodeo MF, Chu Z, Lewis-Gruss S, Freeman NB, Houser T, Delgado M, Hamidi A, Bolliger I, McCusker EK, Emanuel K, Ferreira CM, Khalid A, Haigh ID, Couasnon A, Kopp ER, Hsiang S, Krajewski WF. 2021.** Combined modeling of US fluvial, pluvial, and coastal flood hazard under current and future climates. *Water Resources* 57:e2020WR028673 DOI 10.1029/2020WR028673.
- Beven KJ. 2006.** A manifesto for the equifinality thesis. *Journal of Hydrology* 320(1–2):18–36 DOI 10.1016/j.jhydrol.2005.07.007.

- Blöschl G, Hall J, Viglione A, Perdigão RAP, Parajka J, Merz B, Lun D, Arheimer B, Aronica GT, Bilibashi A, Bohac M, Bonacci O, Borga M, Canjevac I, Castellarin A, Chirico GB, Claps P, Frolova N, Ganora D, Gorbachova L, Gul A, Hannaford J, Harrigan S, Kireeva M, Kiss A, Kjeldsen TR, Kohnova S, Koskela JJ, Ledvinka O, Macdonald N, Mavrova-Guirguinova M, Mediero L, Merz R, Molnar P, Montanari A, Murphy C, Osuch M, Ovcharuk V, Radevski I, Salinas JL, Sauquet E, Sraj M, Szolgay J, Volpi E, Wilson D, Zaimi K, Zivkovic N. 2019. Changing climate both increases and decreases European river floods. *Nature* 573:108–111.
- Chen Z, Goldscheider N. 2014. Modeling spatially and temporally varied hydraulic behavior of a folded karst system with dominant conduit drainage at catchment scale, Hochifien–Gottesacker, Alps. *Journal of Hydrology* 514:41–52 DOI 10.1016/j.jhydrol.2014.04.005.
- Chen J, Zhu X, Vogelmann JE, Gao F, Jin S. 2011. A simple and effective method for filling gaps in Landsat ETM+ SLC-off images. *Remote Sensing of Environment* 115:1053–1064 DOI 10.1016/j.rse.2010.12.010.
- Drew D. 2008. Hydrogeology of lowland karst in Ireland. *The Quarterly Journal of Engineering Geology and Hydrogeology* 41:61–72 DOI 10.1144/1470-9236/07-027.
- Ghasemizadeh RF, Hellweger C, Butscher I, Padilla D, Vesper M, Field M, Alshawabkeh A. 2012. Review: groundwater flow and transport modeling of karst aquifers, with particular reference to the North Coast Limestone aquifer system of Puerto Rico. *Hydrogeology Journal* 20(8):1441–1461 DOI 10.1007/s10040-012-0897-4.
- Gill LW, Naughton O, Johnston PM, Basu B, Ghosh B. 2013. Characterisation of hydrogeological connections in a lowland karst network using time series analysis of water levels in ephemeral groundwater-fed lakes (turloughs). *Journal of Hydrology* 499:289–302 DOI 10.1016/j.jhydrol.2013.07.002.
- Gill LW, Schuler P, Duran L, Johnston PM, Morrissey P. 2020. An evaluation of semi-distributed-pipe-network and distributed-finite-difference models to simulate karst systems. *Hydrogeology Journal* 29:259–279 DOI 10.1007/s10040-020-02241-8.
- Gumbrecht T, Wolski P, Frost P, McCarthy TS. 2004. Forecasting the spatial extent of the annual flood in the okavango delta, botswana. *Journal of Hydrology* 290(3–4):178–191 DOI 10.1016/j.jhydrol.2003.11.010.
- Guo F, Jiang GH, Yuan DX, Polk JS. 2013. Evolution of major environmental geological problems in karst areas of Southwestern China. *Environmental Earth Sciences* 69:2427–2435 DOI 10.1007/s12665-012-2070-8.
- Guzman SM, Paz JO, Tagert MLM. 2017. The use of NARX neural networks to forecast daily groundwater levels. *Water Resources Management* 31(5):1591–1603 DOI 10.1007/s11269-017-1598-5.
- Hadid B, Duviella E, Lecoecuche S. 2020. Data-driven modeling for river flood forecasting based on a piecewise linear ARX system identification. *Journal of Process Control* 86:44–56 DOI 10.1016/j.jprocont.2019.12.007.

- Hartmann A, Goldscheider N, Wagener T, Lange J, Weiler M. 2014.** Karst water resources in a changing world: review of hydrological modeling approaches. *Reviews of Geophysics* **52**:218–242 DOI [10.1002/2013rg000443](https://doi.org/10.1002/2013rg000443).
- Hill CA, Polyak VJ. 2020.** A karst hydrology model for the geomorphic evolution of Grand Canyon, Arizona, USA. *Earth-Science Reviews* **208**:Article 103279 DOI [10.1016/j.earscirev.2020.103279](https://doi.org/10.1016/j.earscirev.2020.103279).
- James G, Witten D, Hastie T, Tibshirani R. 2013.** *An introduction to statistical learning with application in R*. New York: Springer.
- Ji J, Choi C, Yu M, Yi J. 2012.** Comparison of a data-driven model and a physical model for flood forecasting. In: *FRIAR 2012*. DOI [10.2495/FRIAR120111](https://doi.org/10.2495/FRIAR120111).
- Jongman B. 2018.** Effective adaptation to rising flood risk. *Nature Communications* **9**:Article 1986 DOI [10.1038/s41467-018-04396-1](https://doi.org/10.1038/s41467-018-04396-1).
- Koks E. 2018.** Moving flood risk modelling forwards. *Nature Climate Change* **8**:561–562 DOI [10.1038/s41558-018-0185-y](https://doi.org/10.1038/s41558-018-0185-y).
- Kovács A, Sauter M. 2007.** Modelling karst hydrodynamics. In: Goldscheider N, Drew D, eds. *Methods in karst hydrogeology, IAH international contributions to hydrogeology*. Vol. 26. London: Taylor & Francis/Balkema, 65–91.
- Kurtulus B, Razack M. 2007.** Evaluation of the ability of an artificial neural network model to simulate the input–output responses of a large karstic aquifer: the La Rochefoucauld aquifer (Charente, France). *Hydrogeology Journal* **15**:241–254 DOI [10.1007/s10040-006-0077-5](https://doi.org/10.1007/s10040-006-0077-5).
- Lee WK, Tuan Resdi TA. 2016.** Simultaneous hydrological prediction at multiple gauging stations using the NARX network for Kemaman catchment, Terengganu, Malaysia. *Hydrological Sciences Journal* **61**(16):2930–2945 DOI [10.1080/02626667.2016.1174333](https://doi.org/10.1080/02626667.2016.1174333).
- Li J, Hu J-M, Deng W, Huang S-L, Jia H-F, Zhu C-L, Luo H-X. 2013.** Revealing storage-area relationship of open water in ungauged subalpine wetland—Napahai in Northwest Yunnan, China. *Journal of Mountain Science* **10**:553–563 DOI [10.1007/s11629-013-2596-6](https://doi.org/10.1007/s11629-013-2596-6).
- Li J, Hu J-M, Zhang H, Luo H-X, Jia H-F, Zhang K-Q. 2015.** The simulation of water storage fluctuation in ungauged subalpine wetlands—Napahai in Northwest Yunnan, China. *Journal of Natural Resources* **30**:340–349 DOI [10.11849/zrzyxb.2015.02.016](https://doi.org/10.11849/zrzyxb.2015.02.016).
- Long D, Shen Y, Sun A, Hong Y, Longuevergne L, Yang Y, Li B, Chen L. 2014.** Drought and flood monitoring for a large karst plateau in Southwest China using extended GRACE data. *Remote Sensing of Environment* **155**:145–160 DOI [10.1016/j.rse.2014.08.006](https://doi.org/10.1016/j.rse.2014.08.006).
- Malagò A, Efstathiou D, Bouraoui F, Nikolaidis NP, Franchini M, Bidoglio G, Kritsotakis M. 2016.** Regional scale hydrologic modeling of a karst-dominant geomorphology: the case study of the island of crete. *Journal of Hydrology* **540**:64–81 DOI [10.1016/j.jhydrol.2016.05.061](https://doi.org/10.1016/j.jhydrol.2016.05.061).

- Naghbi SA, Ahmadi K, Daneshi A. 2017.** Application of support vector machine, random forest, and genetic algorithm optimized random forest models in groundwater potential mapping. *Water Resources Management* **31(9)**:2761–2775 DOI [10.1007/s11269-017-1660-3](https://doi.org/10.1007/s11269-017-1660-3).
- Napahai Nature Reserve Administration. 2020.** Annual Ecological Monitoring Report of Napa Sea Nature Reserve 2020..
- Noone S, Broderick C, Duffy C, Matthews T, Wilby RL, Murphy C. 2017.** A 250-year drought catalogue for the island of Ireland (1765–2015). *International Journal of Climatology* **37**:239–254 DOI [10.1002/joc.4999](https://doi.org/10.1002/joc.4999).
- Qian K, Mohamed A, Claudel C. 2019.** Physics informed data driven model for flood prediction: application of deep learning in prediction of urban flood development. ArXiv preprint. [arXiv:1908.10312](https://arxiv.org/abs/1908.10312), 34.
- Rencher AC, Schaalje GB. 2008.** *Linear models in statistics*. Hoboken: John Wiley & Sons, Inc.
- Sawaf MBA, Kawanisi K, Jilati MN, Xiao C, Bahreinimotlagh M. 2021.** Extent of detection of hidden relationships among different hydrological variables during floods using data-driven models. *Environmental Monitoring and Assessment* **193**:Article 692 DOI [10.1007/s10661-021-09499-9](https://doi.org/10.1007/s10661-021-09499-9).
- Seleem O, Ayzel G, Souza ACTD, Bronstert A, Heistermann M. 2022.** Towards urban flood susceptibility mapping using data-driven models in Berlin, Germany. *Geomatics, Natural Hazards and Risk* **13(1)**:1640–1662 DOI [10.1080/19475705.2022.2097131](https://doi.org/10.1080/19475705.2022.2097131).
- Spence C, Whitfield PH, Pomeroy JW, Pietroniro A, Burn DH, Peters DL, St-Hilaire A. 2013.** A review of the Prediction in Ungauged Basins (PUB) decade in Canada. *Canadian Water Resources Journal* **38(4)**:253–262 DOI [10.1080/07011784.2013.843867](https://doi.org/10.1080/07011784.2013.843867).
- Sullivan PL, Price RM, Schedlbauer JL, Saha A, Gaiser EE. 2014.** The influence of hydrologic restoration on groundwater-surface water interactions in a Karst Wetland, the Everglades (FL, USA). *Wetland* **34(1 Supplement)**:23–35 DOI [10.1007/s13157-013-0451-8](https://doi.org/10.1007/s13157-013-0451-8).
- Wen L, Macdonald R, Tim M, Hameed T, Saintilan N, Ling J. 2013.** From hydrodynamic to hydrological modelling: investigating long-term hydrological regimes of key wetlands in the macquarie marshes, a semi-arid lowland floodplain in Australia. *Journal of Hydrology* **500**:45–61 DOI [10.1016/j.jhydrol.2013.07.015](https://doi.org/10.1016/j.jhydrol.2013.07.015).
- Windolf J, Thodsen H, Troldborg L, Larsen SE, Bøgestrand J, Ovesena NB, Kronvang B. 2011.** A distributed modelling system for simulation of monthly runoff and nitrogen sources, loads and sinks for ungauged catchments in Denmark. *Journal of Environmental Monitoring* **13**:2645–2658 DOI [10.1039/c1em10139k](https://doi.org/10.1039/c1em10139k).
- Wunsch A, Liesch T, Broda S. 2018.** Forecasting groundwater levels using nonlinear autoregressive networks with exogenous input (NARX). *Journal of Hydrology* **567**:743–758 DOI [10.1016/j.jhydrol.2018.01.045](https://doi.org/10.1016/j.jhydrol.2018.01.045).

- Xu H. 2006.** Modification of normalised difference water index (NDWI) to enhance open water features in remotely sensed imagery. *International Journal of Remote Sensing* 27:3025–3033 DOI [10.1080/01431160600589179](https://doi.org/10.1080/01431160600589179).
- Yang C, Cai X, Wang X. 2018.** Remote sensing of hydrological changes in Tian-e-Zhou Oxbow Lake, an ungauged area of the Yangtze River Basin. *Remote Sensing* 10:Article 27 DOI [10.3390/rs10010027](https://doi.org/10.3390/rs10010027).